Case Studies in Thermal Engineering 60 (2024) 104763

Contents lists available at ScienceDirect

Case Studies in Thermal Engineering

journal homepage: www.elsevier.com/locate/csite

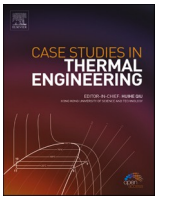

Thermal performance improvement for parabolic trough solar collectors integrated with twisted fin and nanofluid: Modeling and validation

Guoliang Hou [a,*], Anupam Yadav [m,n], Eyhab Ali [b], Youssef Ali Naeem [c], Fadwa Fathallah Ahmed [d], Khursheed Muzammil [e], Khaldoon T. Falih [f], Hussam Abdali Abdulridui [g], Eftikhaar Hasan Kadhum [h], Alaa A. Omran [i], Ahmed Elawady [j,k,l]

[a] *Mathematics School of Changchun Normal University, Changchun, 130032, China*
[b] *Al-Zahraa University for Women, Karbala, Iraq*
[c] *Al-Manara College for Medical Sciences, (Maysan), Iraq*
[d] *Department of Anesthesia Techniques, Al-Noor University College, Nineveh, Iraq*
[e] *Department of Public Health, College of Applied Medical Sciences, Khamis Mushait Campus, King Khalid University, Abha, 62561, Saudi Arabia*
[f] *New Era and Development in Civil Engineering Research Group, Scientific Research Center, Al-Ayen University, Thi-Qar, Iraq*
[g] *Al-Hadi University College, Baghdad, 10011, Iraq*
[h] *National University of Science and Technology, Dhi Qar, Iraq*
[i] *Department of engineering, AL-Nisour University College, Baghdad, Iraq*
[j] *College of technical engineering, the Islamic University, Najaf, Iraq*
[k] *College of technical engineering, the Islamic University of Al Diwaniyah, Iraq*
[l] *College of technical engineering, the Islamic University of Babylon, Iraq*
[m] *Department of Mechanical Engineering, Faculty of Engineering and Technology, Jain (Deemed-to-be) University, Bengaluru, Karnataka, 560069, India*
[n] *Department of Mechanical Engineering, Vivekananda Global University, Jaipur, Rajasthan, 303012, India*

ARTICLE INFO

Keywords:
Parabolic trough solar collector
Twisted insertion
Nanofluids
Thermal performance
Frictional losses
CFD

ABSTRACT

The low thermal efficiency of parabolic trough solar collectors (PTSCs) is a major drawback that has hindered their development as a viable renewable energy resource. Among the available methods to enhance the thermal performance of PTSCs, installing internal fins within the collector tube is one of the most reliable, economical, and straightforward passive techniques. However, while internal fins can significantly improve thermal performance in turbulent flows, they also lead to a substantial increase in pumping work. Here, we demonstrate that with an optimal design of helical fins, the thermal efficiency of PTSCs can be improved without causing significant pressure losses through the receiver tube. The results proved that higher thermal efficiency and lower pressure losses were achieved when annular fins are replaced by an axial helical insert. Installation of a helical fin with 4 turns and a height of 4 mm led to a 4.5 % increase in thermal efficiency (η) while raising the friction factor (f) by 30 %. Optimal performance was observed with helical fins having 10 turns. For instance, at $Re = 10^5$, switching from 16 to 4 turns of 8 mm helical fins resulted in η and Nu enhancements, and f reduction of 1.6 %, 33 % and 64 %, respectively. While these changes were 2.0 %, 55 % and 54 % when n reduced from 16 to 10.

* Corresponding author.
E-mail address: houguoliangcnu@163.com (G. Hou).

https://doi.org/10.1016/j.csite.2024.104763
Received 30 March 2024; Received in revised form 11 June 2024; Accepted 27 June 2024
Available online 4 July 2024

1. Introduction

The quick depletion of fossil fuel reserves alongside escalating environmental concerns have sparked considerable interest in renewable energy sources. Solar energy stands out due to its unparalleled advantages, including its abundant and freely available nature, widespread distribution across the globe, and environmentally friendly characteristics, making it a preferred option. One of the most practical approaches to harnessing solar energy is through its conversion into thermal energy, with concentrated solar power (CSP) technologies being extensively employed. CSP technologies generally fall into two categories: line-focused and point-focused systems [1]. Line-focused CSP systems have seen widespread adoption due to their ability to operate effectively within low and medium temperature ranges, typically between 50 °C and 500 °C. This adaptability has made them a popular choice for harnessing solar energy [2]. Among the various line-focused CSP devices, parabolic trough solar collectors (PTSCs) emerge as the most economically viable systems, particularly for medium temperature applications [4]. PTSCs offer several additional advantages, including high power capacity, long operational life cycles, resilience to moisture, and design flexibility [5]. But on the other hand, because of high investment required for PTSCs, their economic competitiveness is still not satisfactory, where heat loss of PTSCs needs to be significantly reduced [3].

Using nanofluids as the heat transfer medium has been demonstrated as an efficient method to boost the thermal performance of PTSCs [6]. Numerous studies have demonstrated the enhancement of PTSCs performance through the incorporation of nanoparticles into conventional heat transfer fluids like water or oil [7,8]. Nevertheless, the primary effect of adding nanoparticles is to increase the thermal conductivity of the HTF, leading to less evident performance enhancements. Consequently, many studies have shifted their focus to another promising approach: adjusting the configuration of PTSCs, particularly by incorporating inserts, to facilitate strong thermal mixing [9]. In general, the widely reported inserts can be majorly classified into strips and rings, twisted tapes, and wire coils and fins. Liu et al. [10] found that installation of conical strips increases Nusselt number (*Nu*) up to 103 % with the increases in friction factor (*f*) of 17.44 times. Ghasemi and Ranjbar [11] examined the thermal and hydraulic performances of a PTSC constructed with internal porous rings containing holes. Their investigation revealed a notable improvement of up to 1.6 times in the Nusselt number (*Nu*), albeit accompanied by a significant increase of approximately 30–60 times in the friction factor (*f*). In another work [12], the effects of installing internal toroidal rings on the performance of a PTSC, revealing increases of up to 2.3 times in the Nusselt number (*Nu*) and up to 15 times in the friction factor (f) compared to the clean counterpart. These findings clearly indicate that while rings or fillers can substantially enhance the thermal performance of PTSCs, their significant side effects on flow resistance make them unsuitable options.

Internal fins have been widely used to increase the heat transfer through fluid bulk [13,14]. Internal turbulators could improve the efficiency of solar-based energy systems [15,16]. Singh et al. [17] compared the impact of conical fins with protrusion and dimple roughness on heat transfer improvement of heat exchangers. They reported that conical fins with protrusion shape resulted in higher heat transfer coefficient than dimple-shaped fins. Accordingly, the improvement of thermal performance of solar air heaters with dimple-shaped inserts was discussed in Ref. [18]. Insertion of turbulators within the collector tube of PTSCs is an effective method to increase the thermal performance. However, the pressure losses could be significantly high. Zhu et al. [19] reported that annular turbulators increased *Nu* and *f* of a PTSC up to 1.2 times and 1.5 times, respectively. For twisted tapes, the effects of insertion of louvered twisted tapes to a receiver tube under uniform heat flux was studied by Ghadirijafarbeigloo et al. [20]. It was reported that the insertion of louvered twisted tapes increases *Nu* up to 3.5 time, but *f* still faces up to 3 times of increment. Chang et al. [21] examined performance of a PTSC with twisted tapes, and the results show that *Nu* and *f* increase about 3 and 2.5 times, respectively. Zhu et al. [22] assessed performance of a PTSC with twisted wavy tapes, where increments in *Nu* and *f* of 2 and 3 times, respectively, were obtained. Song et al. [23] investigated a PTSC with helical screw-tape inserts and they found that this leads to up to 23 times of increments in *f*. Singh et al. [24] concluded that in comparison with a plain receiver, insertion of twisted fins increased *Nu* and friction factor of PTSCs by 4.3 and 7.3 times, respectively. Mehta et al. [25] proved that twisted tape installation inside the receiver tube of PTSCs increased the energy efficiency and friction losses by 5.3 % and 230 %, respectively. These results clearly show that though relatively smaller than that of rings or fillers, increases in *f* introduced by installation of twisted tapes are still unacceptably high.

For wire coils, Yilmaz et al. [26] reported that they improved *Nu* of a PTSC only up to 1.4 %, while *f* raises up to 11 times. Sahin et al. [27] conducted both experimental and CFD simulations on thermal performance of a PTSC with internal wire coils. They concluded that although wire coils enhance *Nu* up to 2.25 times, *f* increases up to 28 times. For fins, Kursun [28] stated that increments of *Nu* are 25 % and 78 %, respectively, as longitudinal fins with flat and sinusoidal lateral surface were installed through the receiver tube of a PTSC. However, *f* increases up to 4 times. Chakraborty et el [29]. Used a CFD method to investigate the performance of a PTSC integrated with an inner helical coil. They results showed that the thermal energy improved by 32.3 %, while the pumping work increased by 13.0 %.

In summary, strips and rings, twisted tapes, and wire coils and fins have their own strengths and weaknesses on heat transfer and flow resistance for performance of PTSCs. Therefore, a design that can integrate the merits of these types of inserts is favoured. Helical fins, a novel type of fins with the characteristics of rings and wire coils, have been recently been conceptualized to improve performance of PTSCs [30–32]. Jalili et al. [33] showed that insertion of helical baffle inside a tube increase the heat transfer. However, they stated that helix angle significantly affected the pressure losses through the tube. Design parameters of helical fins should be carefully identified to achieve satisfactory thermal and pumping efficiencies for PTCSs. Smaller helical fins may have clear improvement on *Nu*, but *f* may be still too high. As configurations of helical fins are somewhat complicated, using costly and time-consuming experimental approaches may be not a good choice to secure ideal design parameters of helical fins. Computational fluid dynamics (CFD), on the other hand, has shown its capability to expedite design and optimization of inserts for PTSCs [34]. Therefore, in this study, CFD was employed to investigate the effects of helical fins on performance improvement for a PTSC.

Recently, CFD simulation has been used to determine the performance of PTSCs with helical fins. Zaboli et al. [35] used CFD modeling to investigate the effect of helical axial fins on the performance of PTSCs. The maximum thermal efficiency improvement was 21.53 %. However, their model had some limitations, namely the dimensions of the length and diameter of the collector tube were low (2 m and 30 mm, respectively), and a constant heat flux was considered in their simulations. As an important factor, a time-dependant solar heat flux needs to be applied to the model to justify the applicability of the proposed design. Oketola and Mwesigye [36] studied the performance of a PTSC integrated with twisted tape insert using a CFD model. However, the collector was designed for CO_2 as the working fluid. While fluid HTFs are preferred to be used in thermal applications, e.g. heat exchangers and industrial preheating process, due to their higher thermal capacity compared to gases. Here, we designed and modelled a PTSC integrated with an optimized helical insert whose working fluid is Cu-Therminol-VP-1 with a very high specific heat.

In this study, CFD was used to investigate how helical fins could improve performance of a nanofluids-based PTSC. It is worth noting that the nanofluids in this work was carefully selected as mainstream nanofluids suffer the issue of rapid increases in viscosity at relatively high temperature. The nanofluids in our work is Cu-Therminol-VP-1 which does not have much elevation of viscosity as temperature increases to maintain acceptable viscous dissipation. In this following, the studied system and CFD model are briefly described. After experimental validation of the CFD simulations, a detailed presentation of flow and thermal characteristics of the PTSC with helical fin will be given. Finally, a parametric analysis of geometrical variations of the helical fin on heat transfer and pressure loss will be discussed.

2. Physical model

Schematic of the modelled PTSC is shown in Fig. 1, where geometry of the helical fin is defined by its axial length L, thickness b, height c, and number of turns n. It can be seen that the helical fin is attached to inner surface of the receiver tube. Solar radiation comes into the glass envelope and reaches the tube. The HTF flows into the tube from the inlet and out from the outlet to receive heat from the tube inner surface. Detailed information about the design parameters of the proposed PTSC is shown in Table 1.

2.1. Properties of the base fluid

Thermophysical properties of Therminol-VP-1 are considered as functions of temperature [37]. The correlation for specific heat capacity within temperature range of 373.15 K $\leq T \leq$ 698.15 K is:

$$C_{p,b} = 2.125 \times 10^3 - 11.017\,T + 0.049862\,T^2 - 7.7663 \times 10^{-5} T^3 + 4.394 \times 10^{-8} T^4 \quad (\mathrm{J/kgK}) \tag{1}$$

Dynamic viscosity of Thermonol-VP-1 within temperature range of 373.15 K $\leq T \leq$ 698.15 K is:

$$\mu_b = 23.165 - 0.1476\,T + 3.617 \times 10^{-4} T^2 - 3.9844 \times 10^{-7} T^3 + 1.6543 \times 10^{-10} T^4 \quad (\mathrm{mPa.s}) \tag{2}$$

Thermal conductivity of Thermonol-VP-1 within temperature range of 373.15 K $\leq T \leq$ 698.15 K is:

$$\lambda_b = 0.1464 + 2.0353 \times 10^{-5} T - 1.9367 \times 10^{-7} T^2 + 1.0614 \times 10^{-11} T^3 \quad (\mathrm{W/mK}) \tag{3}$$

Density of Thermonol-VP-1 within temperature range of 373.15 K $\leq T \leq$ 698.15 K is:

$$\rho_b = 1.4386 \times 10^3 - 1.87115\,T + 2.737 \times 10^{-3} T^2 - 2.3793 \times 10^{-6} T^3 \left(\mathrm{kg/m^3}\right) \tag{4}$$

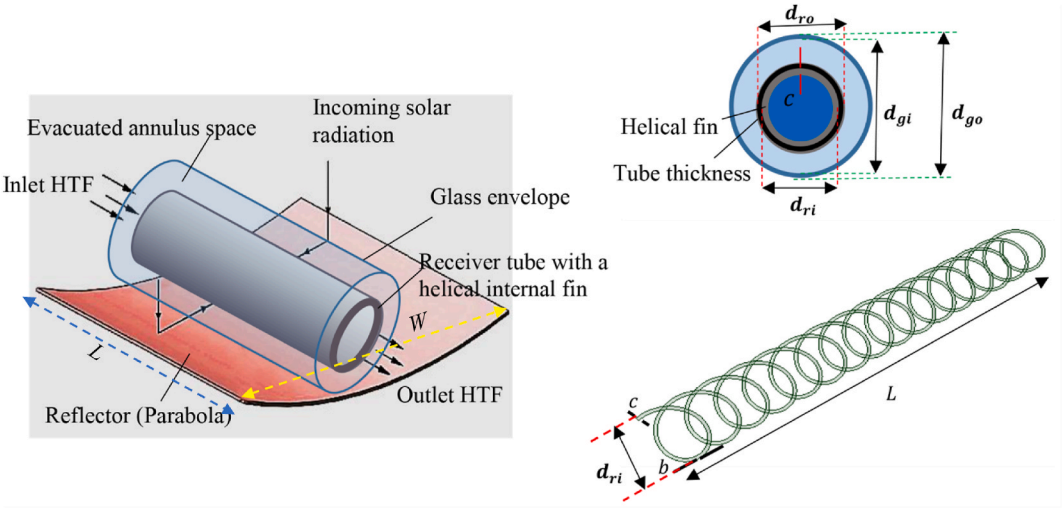

Fig. 1. Illustration of different elements of the PTSC with helical fins.

Table 1
Design parameters of the modelled PTSC with a twisted insertion.

Parameter	Value
Internal diameter of the collector, d_{ri} (mm)	76
External diameter of the collector, d_{ro} (mm)	80
Inner diameter of the glass envelope, d_{gi} (mm)	120
Outer diameter of the glass envelope, d_{go} (mm)	125
Height of the fin, c (mm)	4, 8, 12
Parabolic concentrator length, W (m)	9.0
Collector tube length, L (m)	5.0
Number of turns of the fin, n	4, 10, 16
Thickness of the fin, b (mm)	2
Absorption coefficient of the collector, α	0.96
Transmission coefficient of the glass wrap, τ_g	0.97
Reflection coefficient of the collector, Γ	0.96
Emission coefficient of the transparent wrap, ξ_g	0.86
Feeding temperature of heat transfer oil, T_{in} (K)	400
Solar heat flux, I_b (W.m^{-2})	1000

2.2. Properties of the nanoparticles

Density and thermal expansion coefficient of the Cu nanoparticles are taken as 8933 kg/m^3 and 1.67 K^{-1}, respectively [38]. In addition, specific heat capacity and thermal conduction coefficient of the Cu nanoparticles are given as [39]:

$$C_{p,p} = 285.8 + 0.44631\ T - 5.2054 \times 10^{-4} T^2 + 2.3958 \times 10^{-7} T^3\ (\mathrm{kJ/kgK}) \tag{5}$$

$$\lambda_p = 441.6 - 0.17119\ \mathrm{T} + 1.5446 \times 10^{-4} T^2 - 7.2917 \times 10^{-8} T^3 \quad (\mathrm{W/mK}) \tag{6}$$

2.3. Properties of the nanofluids

For the mixture of Therminol-VP-1 and Cu nanoparticles, its thermophysical properties are listed in Table 2. It is worth noting that the Cu nanoparticles and Therminol-VP-1 are in thermal equilibrium.

3. Conservation equations

Here, the steady-state momentum and energy conservation equations were employed to model flow and heat transfer. The three-dimensional governing equations for mass and momentum conservation are:

$$\frac{\partial(\rho_m \overline{u}_i)}{\partial x_i} = 0 \tag{7}$$

$$\frac{\partial}{\partial x_j}\left(\rho_m \overline{u}_i \overline{u}_j\right) = -\frac{\partial P}{\partial x_i} + \frac{\partial}{\partial x_j}\left[\mu_m\left(\frac{\partial \overline{u}_i}{\partial x_j} + \frac{\partial \overline{u}_j}{\partial x_i}\right) - \frac{2}{3}\mu_m \frac{\partial \overline{u}_i}{\partial x_i}\delta_{ij} - \rho_m \overline{u_i u_j}\right] + (\rho\beta)_m (T - T_0)\,\vec{g} \tag{8}$$

where $\overline{u}_i$ represents time-averaged velocity component in i direction. Besides, P, β, T_0 and subscript m denote time-averaged pressure, thermal expansion coefficient, reference temperature and mixture of the HTF, respectively. The term $\rho_f \overline{u_i u_j}$ represents the Reynolds stress and is expressed as [39]:

Table 2
Effective thermophysical properties of the Cu -Therminol-VP-1 nanofluids.

Properties	Definitions of parameters	Ref.
$\rho_m = (1-\varphi)\rho_b + \varphi\rho_p$	φ: Volume fraction	[40]
$(\rho\beta)_m = (1-\varphi)\rho_b\beta_b + \varphi\rho_p\beta_p$	β: Thermal expansion coefficient	[41]
$\mu_m = \mu_b \Big/ \left[1 - 34.87\left(\frac{d_p}{d_b}\right)^{-0.3} \varphi^{1.03}\right]$	d_p: Nanoparticle diameter d_b: Equivalent diameter of the base fluid molecule	[42]
$\lambda_m = \lambda_b\left[1 + 4.4 Re_B^{0.4}\, Pr^{0.66}\left(\frac{T}{T_{br}}\right)^{10}\left(\frac{\lambda_p}{\lambda_b}\right)^{0.03}\varphi^{0.66}\right]$	k_B: Boltzmann's constant Pr: Prandtl number Re_B: Nanofluids Reynolds number u_B: Nanoparticle Brownian velocity	[42]
$Re_B = \frac{\rho_b u_B d_p}{\mu_b}$		
$u_B = \frac{2k_B T}{\pi\mu_b d_p^2}$		
$Pr = \frac{C_{p,b}\mu_b}{\lambda_b}$		
$C_{p,m} = \left[(1-\varphi)\rho_b C_{p,b} + \varphi\rho_p C_{p,p}\right]/\rho_m$		[43]

$$-\rho_m \overline{u_i}\overline{u_j} = \mu_m\left(\frac{\partial \overline{u_i}}{\partial x_j}+\frac{\partial \overline{u_j}}{\partial x_i}\right)-\frac{2}{3}\left(\rho_m k+\mu_t\frac{\partial \overline{u_k}}{\partial x_k}\right)\delta_{ij} \tag{9}$$

where μ_t represents turbulent viscosity which is given as:

$$\mu_t = \rho_m C_\mu \frac{k^2}{\varepsilon} \tag{10}$$

where the coefficient C_μ is taken 0.09. Besides, in Eq. (8), δ_{ij} and k stand for deformation rate of the fluid elements and turbulent kinetic energy, respectively, which are expressed as:

$$\delta_{ij} = \frac{1}{2}\left(\frac{\partial \overline{u_i}}{\partial x_j}+\frac{\partial \overline{u_j}}{\partial x_i}\right) \tag{11}$$

$$k = \frac{1}{2}\left(\overline{u_x^2}+\overline{u_y^2}+\overline{u_z^2}\right) \tag{12}$$

In this study, the realizable k-ε turbulent model was used to model turbulent flow inside the receiver tube, where transport equations for k and turbulent dissipation rate ε are given as:

$$\frac{\partial}{\partial x_j}\left(\rho_m k \overline{u_j}\right) = \frac{\partial}{\partial x_j}\left[\left(\mu_m+\frac{\mu_t}{\sigma_k}\right)\frac{\partial k}{\partial x_j}\right]+G_k-\rho_m\varepsilon \tag{13}$$

$$\frac{\partial}{\partial x_j}\left(\rho_m \varepsilon \overline{u_j}\right) = \frac{\partial}{\partial x_j}\left[\left(\mu_m+\frac{\mu_t}{\sigma_\varepsilon}\right)\frac{\partial \varepsilon}{\partial x_j}\right]+\rho_m\varepsilon C_1 S-\rho_m C_2\frac{\varepsilon^2}{k+\sqrt{\nu\varepsilon}} \tag{14}$$

where σ_k and σ_ε are turbulent Prandtl number for k and ε, respectively, which are taken as 1 and 1.2. The constant coefficients C_1, S, and C_2 are given as:

$$C_1 = max\left[0.43, \frac{\Lambda}{\Lambda+5}\right], \Lambda = S\frac{k}{\varepsilon}, S = \sqrt{2\overline{S_{ij}S_{ij}}}, C_2 = 1.9 \tag{15}$$

where S_{ij} stands for linear deformation rate of the HTF. Moreover, G_k denotes production of turbulent kinetic energy that is given as:

$$G_k = \mu_t S^2 \tag{16}$$

The energy equation of HTF is given as:

$$\frac{\partial}{\partial x_j}\left(\rho_m \overline{u_j} C_{p,m} T\right) = \frac{\partial}{\partial x_j}\left(\lambda_m\frac{\partial T}{\partial x_j}+\frac{\mu_t}{\sigma_{h,t}}\frac{\partial\left(C_{p,m}T\right)}{\partial x_j}\right)+\overline{u_j}\frac{\partial P}{\partial x_j}+\frac{\partial \overline{u_i}}{\partial x_j}\left[\mu_m\left(\frac{\partial \overline{u_i}}{\partial x_j}+\frac{\partial \overline{u_j}}{\partial x_i}\right)-\frac{2}{3}\mu_m\frac{\partial \overline{u_i}}{\partial x_i}\delta_{ij}-\rho_m\overline{u_i u_j}\right] \tag{17}$$

where $\sigma_{h,t}$ represents the turbulent Prandtl number and is taken 0.85. In addition, radiative and wind-driven forced convective heat loss from the glass cover were calculated as [44]:

$$\dot{Q}_{loss} = \pi d_{go} L h_w\left(T_{go}-T_a\right)+\xi_g\pi d_{go}L\sigma\left(T_{go}^4-T_{sky}^4\right) \tag{18}$$

where ξ_g, h_w, T_{sky} and T_{go} represent the emission coefficient of the transparent glass wrap, heat transfer coefficient for convection upon glass wrap, temperature through the external surface of the glass wrap, and sky temperature, respectively. In this work, $h_w = V_w^{0.58}d_{go}^{-0.42}$ and $T_{sky} = 0.0552T_a^{1.5}$ were taken, respectively, where $T_a = 300\,K$ and $V_w = 2\,ms^{-1}$ are ambient temperature and wind speed, respectively.

3.1. Boundary conditions

At the inlet, the following conditions are given:

$$u_i(x,y,0) = 0, u_j(x,y,0) = 0, u_k(x,y,0) = W_{in}, T(x,y,0) = T_{in} \tag{19}$$

where i, j and k represent the directions of x, y and z, respectively. At the outlet, the fully developed flow condition was assumed to be $\partial u_i/\partial z = \partial u_j/\partial z = \partial u_k/\partial z = \partial T/\partial z = 0$. For the vacuumed region between the glass envelope and outer wall of the receiver tube, a non-uniform heat flux q_w was assigned to the glass cover:

$$q_w = \alpha_a \tau_g q^{'} \tag{20}$$

Where τ_g and α_a are transmission coefficient of the glass wrap and absorption coefficient of the collector, respectively. $q^{'}$ is the non-uniform heat flux reflected from the parabolic concentrator, as illustrated in Fig. 2(a). Fig. 2(b) shows different conjugate heat transfer processes between different regions, e.g., between HTF and fin, HTF and inner wall of the receiver tube, and air and outer wall of the

receiver tube.

3.2. Dimensionless parameters

Several dimensionless parameters were introduced to better assess performance and quantify the influence of operating conditions. Nusselt number of the HTF is defined as:

$$Nu = \frac{hD_h}{\lambda_m} \tag{21}$$

where h and D_h stand for average heat transfer coefficient between inner wall of the tube and HTF, and hydraulic diameter of the receiver tube, respectively. h is obtained as [45]:

$$h = \frac{q}{(T_{wall} - T_{fluid})} \tag{22}$$

where T_{wall}, T_{fluid} and q are average temperature of inner wall of the receiver tube, temperature of HTF in the vicinity of the wall and heat flux on the tube wall, respectively. Reynolds number of the flow is defined as:

$$Re = \frac{\rho_m W_{in} D_h}{\mu_m} \tag{23}$$

f is defined as [46]:

$$f = \frac{2\Delta P D_h}{L\rho_m W_{in}^2} \tag{24}$$

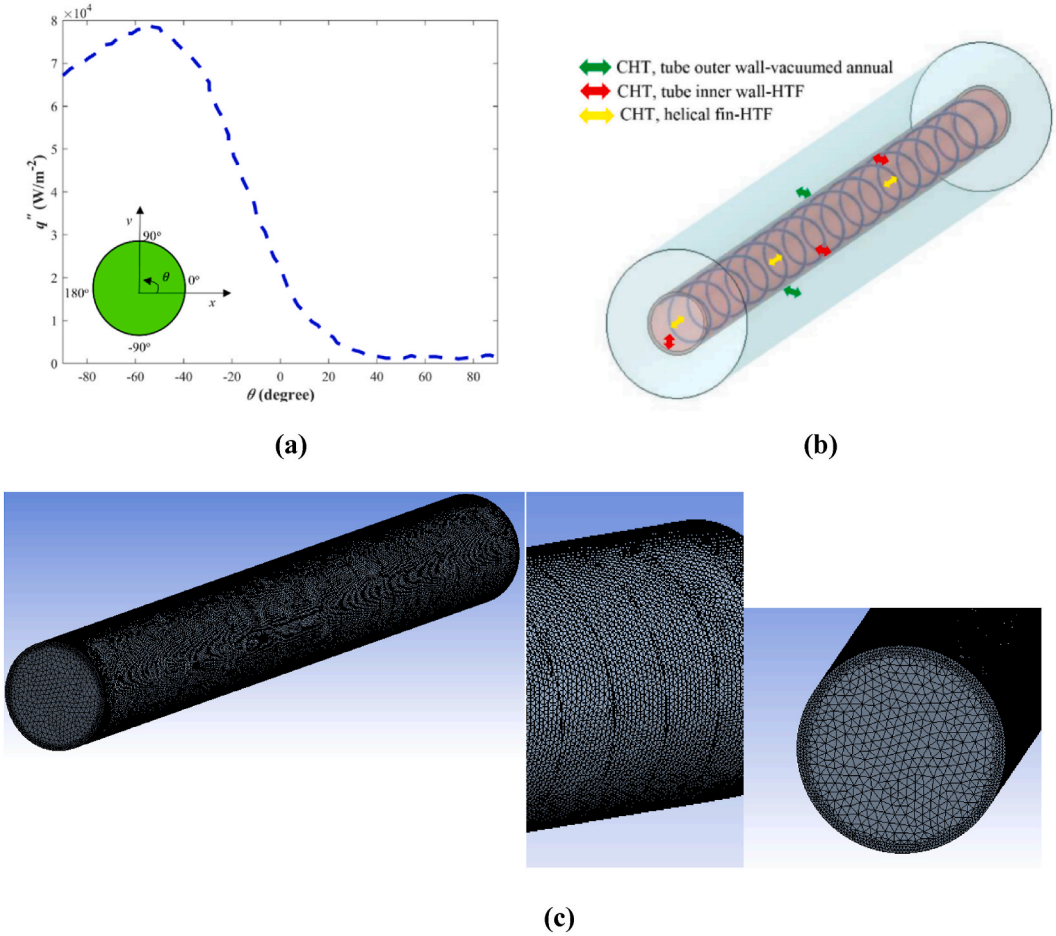

Fig. 2. (a) Concentrated solar flux reflected from the parabolic concentrator to the glass wrap; (b) different conjugate heat transfer processes in the PTSC; (c) Mesh through the receiver tube with a helical fin with 16 turns.

where ΔP stands for overall pressure drop. Efficiency of the PTSC is defined as [47]:

$$\eta = \frac{\dot{m}\overline{C}_{p,m}\left(T_{fluid,out} - T_{in}\right)}{I_b A_{ap}} \tag{25}$$

where $\dot{m}$, T_{in}, $T_{fluid,out}$, and A_{ap} are mass flow rate of the nanofluid, inlet temperature, average outlet temperature, and the aperture normal surface area, in order.

4. Numerical approach

The conservation equations of the model are solved through the finite volume scheme [48] using the ANSYS Fluent® software. Radiation heat through the evacuated region between the glass wrap and the collector was modelled using discrete ordinates method [49]. For the convergence criteria, residuals of continuity, momentum, turbulent kinetic energy, and turbulent dissipation rate were taken 10^{-5}. Moreover, for the energy equation, residual was set to 10^{-7}.

4.1. Mesh refinement and validation

Physical domain of the PTSC was discretised using unstructured tetrahedral meshes. In the generated three-dimensional mesh system, near outer and inner walls of the receiver tube as well as the helical fin, 5 prism layers were generated to capture the velocity and thermal boundary layers. Besides, to capture small-scale eddies, the grid cells were fine enough in the radial direction inside the receiver tube. To evaluate mesh density and determine the most optimized mesh that guarantees both quality and computational cost, a case with a fin of 16 turns and height of 12 mm was selected. For this case, the grid refinement test was carried out for the following operating conditions: $Re = 5 \times 10^6$, $\varphi_{Cu} = 0.04$, and $T_{in} = 400$ K. The results of mesh refinement test are listed in Table 3. It can be seen that the meshed model with about 6.6 million cells provides reliable results with an optimum computational cost.

To check validity of the CFD simulations, performance of a PTSC with Cu-Therminol®VP-1 nanofluids was simulated. Besides, the transparent wrap was in exposure to a transient concentrated solar flux like the current model (see Fig. 2(a)). CFD results were compared with those presented by Mwesigye et al. [39]. Fig. 3 shows the results of validation for both heat transfer coefficient and pumping work. As observed from Fig. 3, the highest errors for h and $\Delta P/L$ are 5.1 % and 7.5 %, which proves that the employed CFD model can give reasonable predictions.

5. Results and discussions

Here, performance of the PTSC with helical fin and Cu-Therminol®VP-1 nanofluids was investigated. First, thermal and hydraulic behaviours of the PTSC with helical fin whose height and number of turns are 4 mm and 4 were compared with the PTSC with annular fin and without fin. Then, performance of the PTSC with different configurations of helical fin were compared.

5.1. The impact of helical fin

Under $Re = 3 \times 10^5$, performance of the PTSC without internal fin was compared with those composed of annular and helical fins. φ_{Cu} was taken to be 0.04. Fig. 4 shows the comparison of Nu, f, and η among different PTSCs. It can be seen that, when helical fin is installed inside the receiver, both Nu and η increase obviously. However, the increments of Nu and η are much lower for annular fin. Indeed, insertion of the helical fin improves axial forced convection within the HTF due to the generation of both radial and axial flows and turbulent eddies. However, for the PTSC with annular fin, turbulent eddies resulted from fluid-fin interactions increase pressure loss very heavily. Thus, qualitatively to say, helical fin can significantly improve heat transfer while not introducing much extra work on pumping.

Fig. 5 shows contours of temperature, stream-wise velocity, radial velocity, and turbulent intensity for the PTSC without fin, with annular fin and helical fin at $Re = 3 \times 10^5$. It can be seen that for helical fin, swirl flows improve turbulent mixing and heat transfer from bottom surface of the tube wall (this area has the maximum temperature) to the whole fluid regions, especially those in the vicinity of top wall. Therefore, across the central x-z and y-z planes, the helical fin stimulates swirl flows that trigger to heat distribution through the whole domain including the upper regions. While annular fin just increases temperature of the bottom areas by transferring heat from bottom of the tube wall that is exposed to concentrated solar flux. For annular fin, strong turbulent vorticities are generated near the fin by which boundary layer near the tube wall becomes thinner, and therefore thermal resistance reduces. This provides better heat transfer from the tube wall to bottom regions of the annular fin, while heat transfer through the upper fluid bulk is very weak. This can explain why Nu with the helical fin is significantly higher than that of the annular fin.

According to Fig. 5, for the annular fin, secondary flows are significantly stronger, though they are limited to narrower areas. On

Table 3
Mesh resolution test for the PTSC with helical fin and Cu-Therminol®VP-1 nanofluids.

Grid number	Nu ($Wm^{-2}K^{-1}$)	Nu variation (%)	f	f variation (%)
3682387	61231	1.47	0.2892	5.59
4854364	61857	0.46	0.2811	2.62
6649983	62130	0.021	0.2742	0.11
7532671	62143	Baseline	0.2739	Baseline

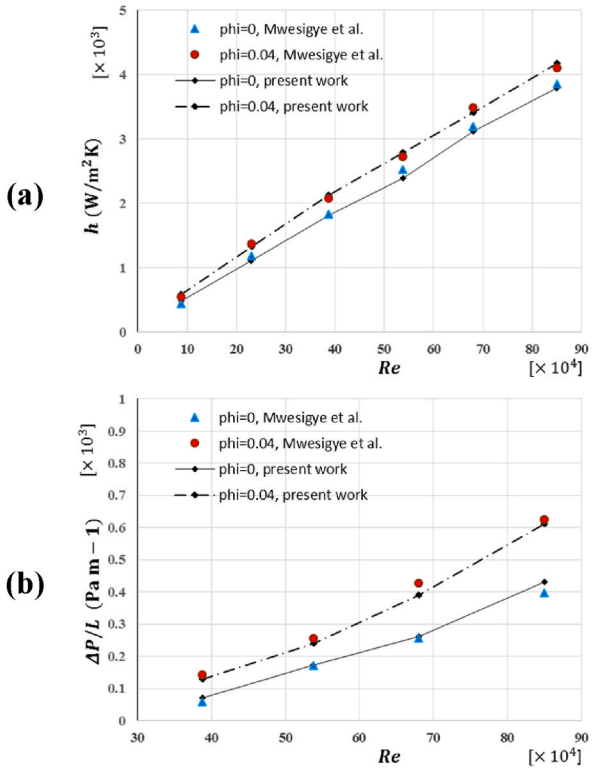

Fig. 3. Validation of the results obtained from CFD simulations compared to the experimental results measured by Mwesigye et al. [39] for a PTSC in which Cu nanoparticle-thermal oil mixture acts as the HTF: (a) heat transfer coefficients and (b) pressure drops per length for T_{in} = 600 K.

the other hand, secondary flows near the helical fin are more extended and can efficiently transfer heat from the fin to the HTF bulk. For the annular fin, secondary flows from face-to-face surfaces, e.g., the left and right fin surfaces, are on opposite directions that confine turbulent mixing and significantly increase pressure loss. While for the helical fin, directions of the secondary flows generate swirl flows. For the helical fin, the magnitude of z-directional velocity is lower since higher portion of the kinetic energy turns to secondary flows. In addition, for the annular fin, the opposite secondary flows from face-to-face fin surfaces result in strong streamwise velocity in the clean regions near centre of the receiver tube. In other words, the HTF bulk in the vicinity of face-to-face fin surfaces are pushed towards the central line by strong opposite secondary flows. Also, there are backward z-directional flows near the annular fin that significantly increase friction factor. Finally, the magnitude of radial velocity inside absorber of the PTSC without fin is about 1000 times lower than that with the helical fin. As a result, heat transfer between collector inner surface and the HTF is significantly weaker. Based on contours of the turbulent intensity, for the PTSC with helical fin, strong turbulent motions appear through the whole domain by which thermal mixing is improved.

Fig. 6 shows streamlines within receiver tube of the PTSC with no fin, annular fin, and helical fin. It is clear that for the PTSC without fin, the streamlines are straight because of weak radial velocity and turbulent intensity (see Fig. 5). On the other hand, for the receiver tube with annular fin, the strong turbulent motions are confined near wall of the fin. But for the PTSC with helical fin, there are strong swirl flows which improve heat transfer within the HTF.

5.2. *The effects of geometry of helical fin*

From the above comparisons, thermal performance of the PTSC with helical fin is significantly higher than that of the PTSC with no fin or annular fin, and the pumping work is considerably lower. To achieve optimal thermal and hydraulic performances, the effects of geometrical configuration of helical fin on efficiency of PTSCs are discussed. Here, c = 4, 8, and 12 mm as well as n = 4, 10, and 16 were chosen. The comparisons are made for $Re = 3 \times 10^4$, 10^5, 3×10^5, 10^6, and 5×10^6. Fig. 7 illustrates the dependence of Nu on Re for different fin configurations. It can be seen that at $Re < 10^6$, for a specific fin height, the highest Nu belongs to the fin with 10 turns. Compared with that with 4 turns, radial velocity is high enough to efficiently transfer solar heat from the receiver wall to the HTF bulk for the fin with 10 turns. In this case, circular flows and turbulent eddies near fin are not too high to suppress axial forced convection. On the other hand, when n increases to 16, large-scale eddies suppress forced convection in z direction so that radial convective heat transfer between the inner wall and HTF is mainly limited to the regions near inner wall. Therefore, heat is not efficiently transferred to the HTF bulk towards the axial direction of tube. For the effects of fin height, heat transfer coefficient increases with the increases in fin height. For instance, at $Re = 3 \times 10^5$ and n = 4, as c increases from 4 mm to 12 mm, Nu increases by 7.3 %. The reason is that larger fin can provide stronger axial forced convection, and more thermal energy is carried to the HTF bulk via both radial and axial flow

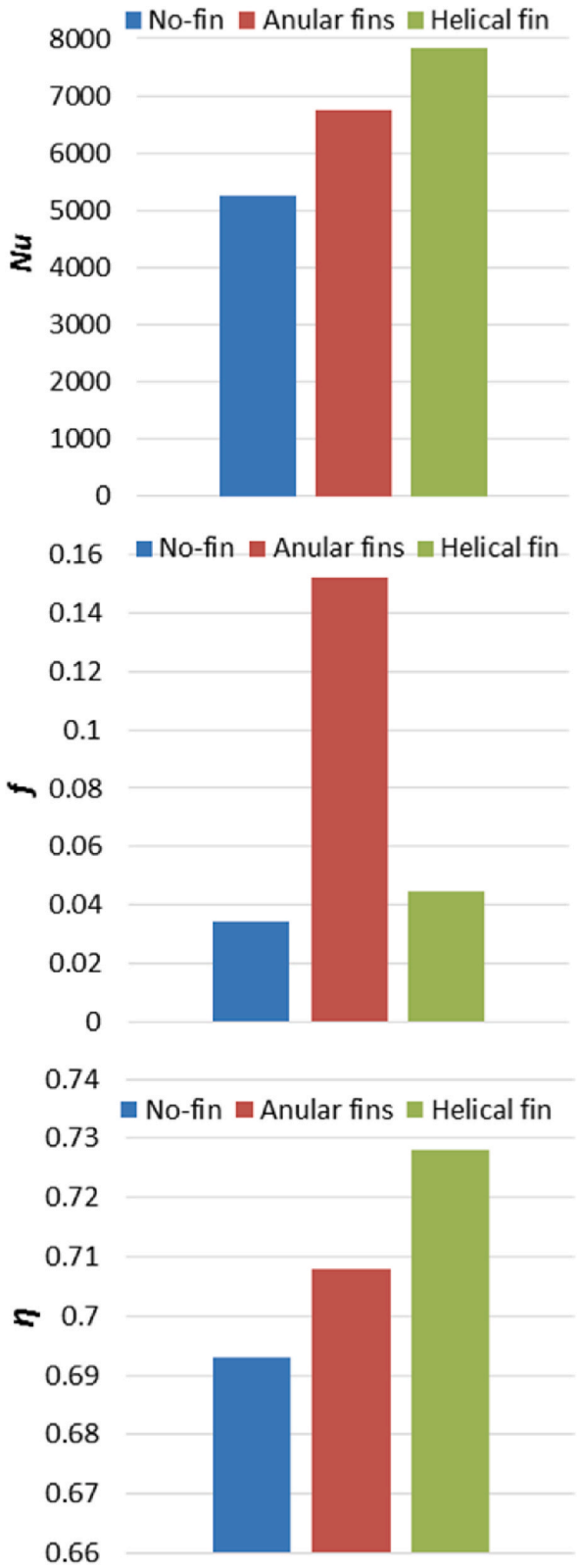

Fig. 4. Comparison of *Nu*, *f*, and η among the PTSC without fin, with annular fin, and helical fin under the condition of $T_{in} = 400$ K, $Re = 3\times 10^5$ and $\varphi_{Cu} = 0.04$.

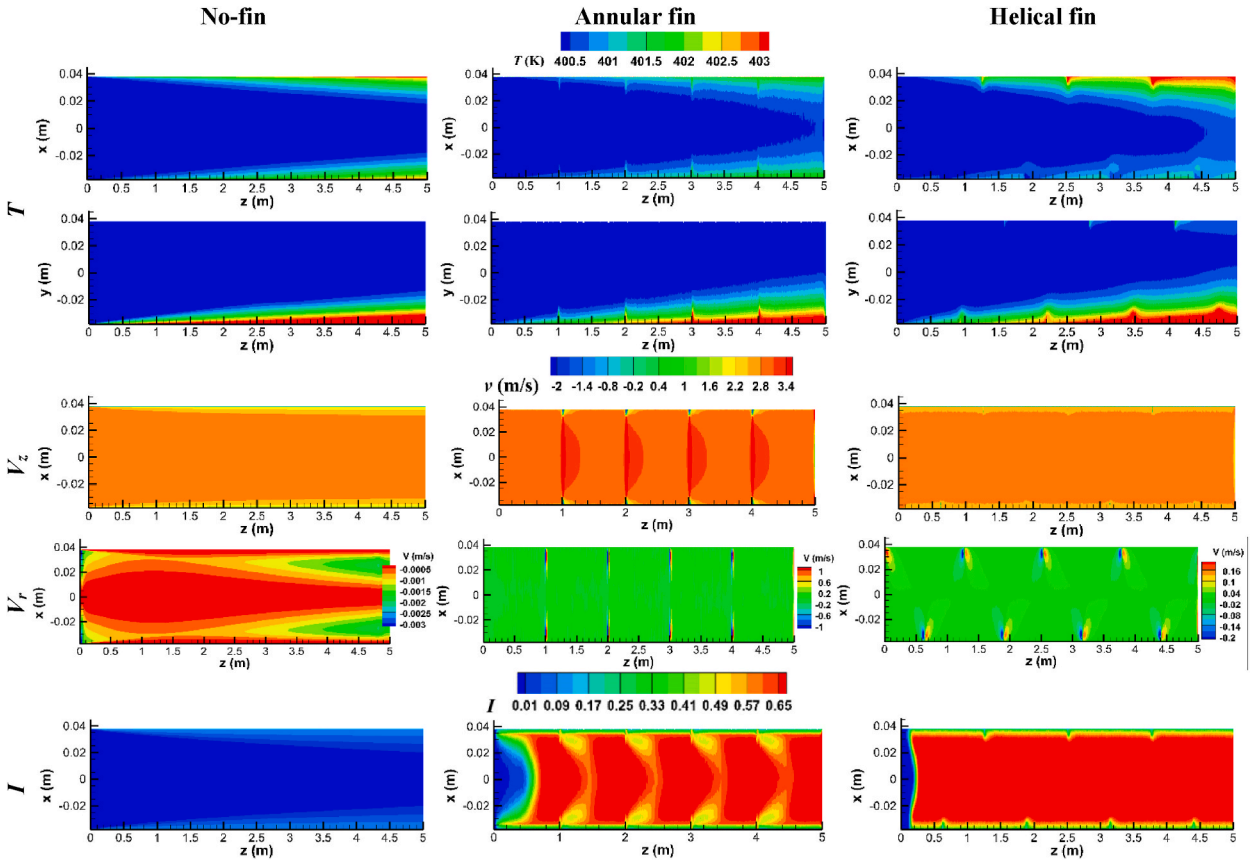

Fig. 5. Contours of temperature, axial and radial velocities, and turbulent intensity distributions through the central *y*-*z* (front view) and *x*-*z* (top view) planes of receiver tube for the PTSC with no fin, annular fin, helical fin. The operating conditions are $T_{in} = 400$ K, $Re = 3 \times 10^5$, and $\varphi_{Cu} = 0.04$.

motions. In this case, circular motions and turbulent eddies near the fin transfer heat from the receiver wall to the inside more efficiently.

Fig. 8 shows the variation of f with c and n. It can be seen that the helical fin with 16 turns generates the highest pressure loss. For example, at $Re = 10^5$ and $c = 8$ mm, f of the fin with 16 turns is 2.2 times higher than that with 10 turns. The reason is that stronger circulations and reverse flows are generated alongside the fin by more turns. These eddies enhance f within the HTF since higher portion of fluid's kinetic energy is devoted to turbulent structures. As c increases, f increases because height of fin plays the major role in determining hydrolic performance. The reason can be explained as follows. For 4 turns, f always decreases with the increases in Re. However, for the cases with 10 and 16 turns, as Re increases, f becomes lower as $Re < 10^6$; while, at $Re = 5 \times 10^6$, f experiences an acute increment. The reason may be ascribed to

Fig. 9 shows the effects of Re on η for different n and c. It can be seen that for all Re, the helical fin of $n = 10$ and $c = 12$ mm provides the highest thermal efficiency. For Re values of 3×10^4 and 10^5, the highest thermal efficiencies belong to cases with 10 turns and higher heights followed by cases with $n = 4$ and $h = 12$, 8 and 4 mm, respectively. For example, in $Re = 10^5$, for cases of $h = 8$ mm, when the number of fin turns changes from $n = 16$ to $n = 4$ and $n = 10$, the η incements are 1.6 % and 2.0 %, respectively. For a Re range of 3×10^4 to 10^6, cases with turn number of $n = 16$ poses the lowest η values. The reason is that at lower Re, for cases with 16 turns the streamwise velocity is not high enough to transfer the radial movements toward the z direction. Therefore, the absorbed solar heat is mainly transferred to the HTF bulk close to the receiver wall (not the central region of HTF). In other words, the distance between helical rings is too low so that axial forced convection near fin is confined to the areas between side walls of two adjacent helical rings. On the other hand, for $Re = 3 \times 10^4$ and 10^5 and $n = 10$, the radial HTF movements and eddies near the fin walls efficiently transfer the heat from the receiver wall to the fluid bulk. Therefore, the axial forced convective heat transfer conveys the heat upwards the stream. For $Re = 3 \times 10^5$ and 10^6, cases of $n = 10$ and $h = 12$ and 8 mm pose the highest thermal efficiencies. For $n = 4$ and $h = 12$ mm, η is higher than the case of $n = 10$ and $h = 4$ mm since the radial forced convection is stronger and the axial velocity is high enough to effectively transfer the heat towards the receiver length. For $Re = 5 \times 10^6$ and $n = 16$, the heat transfer coefficient enhancement results in huge increment in the thermal efficiency. In these cases, the streamwise velocity is strong enough to convey heat towards the axial direction. Therefore, a large portion of generated circular flows and turbulent eddies are not just confined to the side walls of two adjacent helical rings.

Fig. 10 depicts the average temperature on outer wall of the receiver tube (T_w) for different Re and fin configurations. The cases

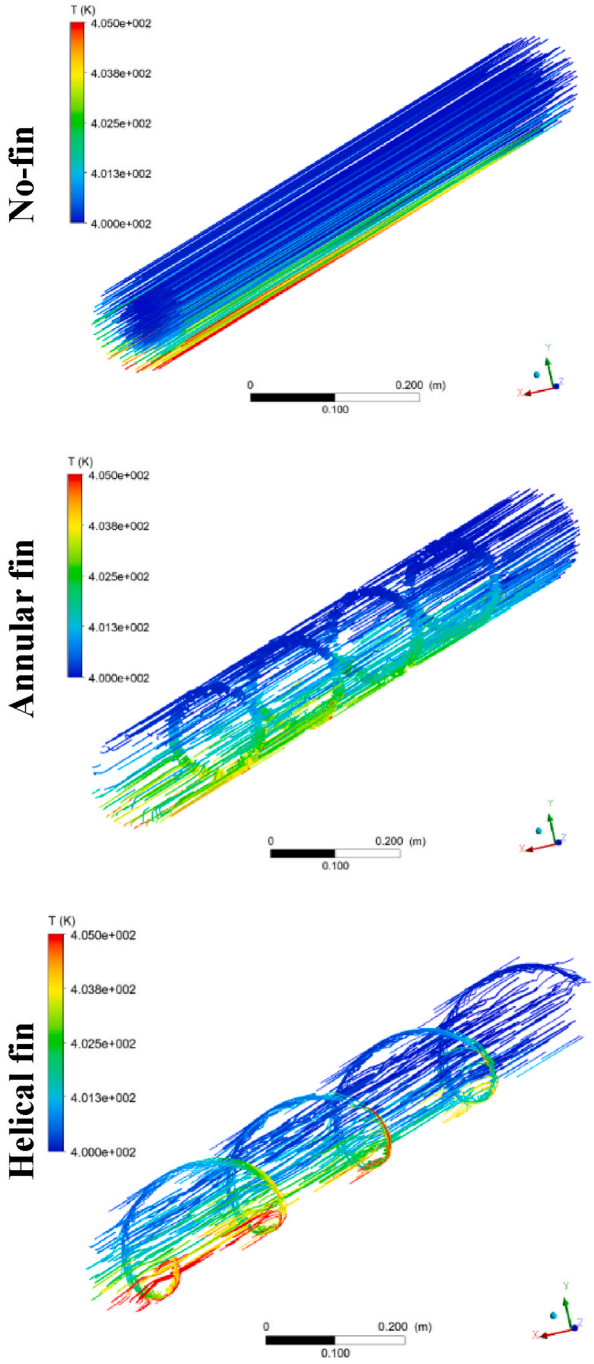

Fig. 6. Streamlines inside receiver tube for the PTSC with no fin, annular fin, helical fin at $T_{in} = 400$ K, $\varphi_{Cu} = 0.04$, and $Re = 3 \times 10^5$.

with higher thermal efficiencies pose lower T_w since larger portion of heat that is absorbed by the collector wall is transferred to HTF. In addition, as Re increases, T_w and its growth rate decrease. The reason is that for higher Re, streamwise forced convection is strong enough to carry the total solar energy that is absorbed by the receiver tube, with just a small temperature difference between the inlet and outlet.

To have a better insight into forced convective heat transfer within the receiver tube, the effects of fin configuration on streamline patterns at $Re = 10^5$ are shown in Fig. 11. According to the figure, for $n = 4$, radial forced convection is weaker than the cases of $n = 10$ and 16. In this case, heat transfer from the receiver wall does not widely goes through the central regions by turbulent motions. But comparatively more uniform temperature distribution across the fin provides efficient heat transfer from the receiver tube wall to the HTF bulk for not only the bottom half cylinder but also the upper one. On the other hand, for $n = 10$, turbulent eddies are generated

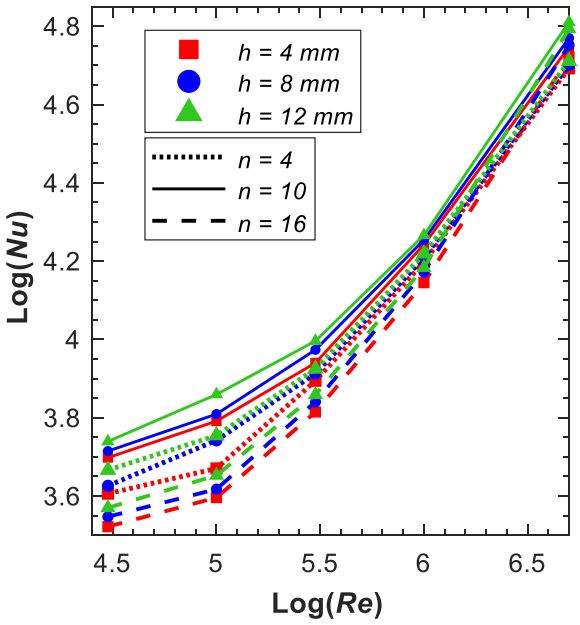

Fig. 7. Changes in the averaged Nusselt number with height and number of turns of the inner fin with respect to *Re*.

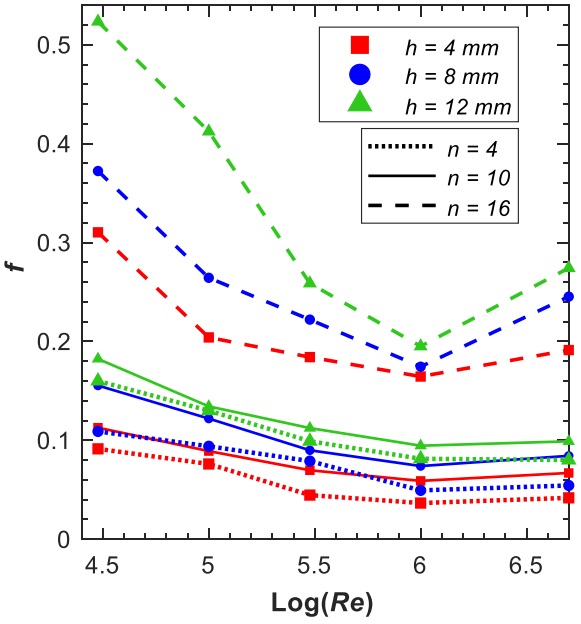

Fig. 8. The impacts of the number of turns and height of fin on *f* of the receiver at different *Re*.

near the fin and the circular flows efficiently transfer heat to both radial and axial directions. As a result, for helical fins with 10 turns, higher thermal efficiency is achieved without huge pressure loss. For $n = 16$, turbulent eddies generated near the fin are so strong. However, because of moderate streamwise velocity, these turbulent structures are confined to the areas near the fin. As a result, heat transfer from the receiver tube to the HTF is suppressed. In this case, f is considerably higher than the cases of $n = 4$ and 10. However, as *Re* increases, streamwise forced convection is high enough to extend the turbulent circular flows towards z direction. Therefore, both axial and radial forced convective flows guarantee a better thermal performance. In addition, for all numbers of turns, the enhancement of c extends turbulent motions to wider areas within the receiver tube, and consequently, improves heat transfer.

Fig. 12 shows the effects of c on temperature contours across the absorber outer wall and helical fin as well as streamlines for $n = 10$ and $Re = 3 \times 10^5$. It can be seen that, for a higher fin, the range of temperature on the collector wall is lower due to better heat transfer

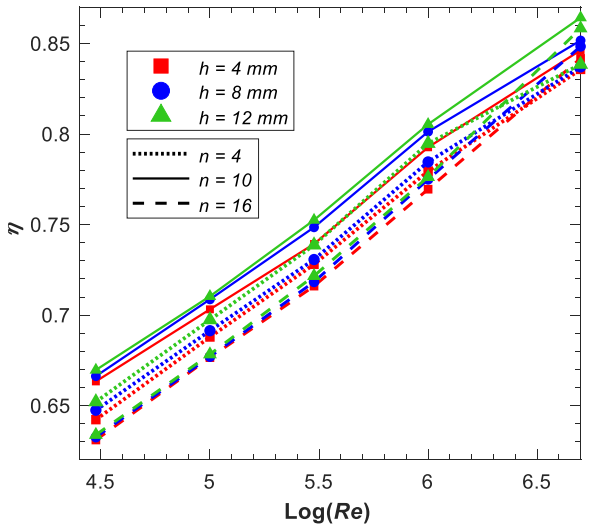

Fig. 9. The effects of Re on η for different number of turns and height of the fin.

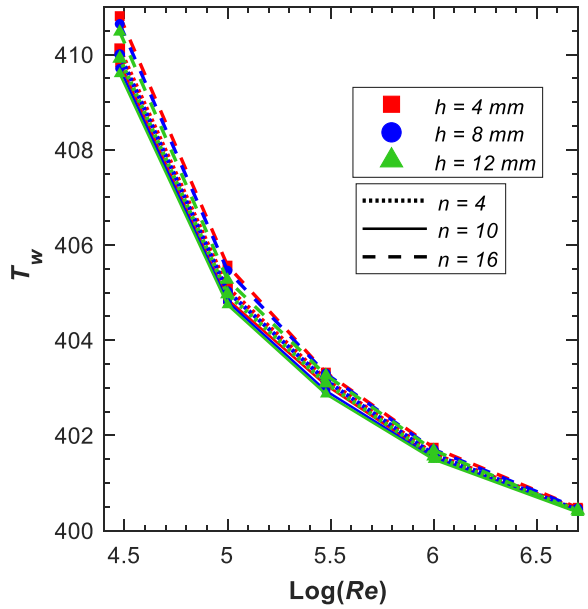

Fig. 10. Changes of averaged temperature of outer wall of the collector with respect to Reynolds number for different fin configurations.

from the absorber to HTF. Besides, temperature through higher fin is lower because radial and axial forced convections from the fin to HTF are amplified with the increment of *h*. For streamline patterns, it can be inferred that for a higher fin, the central regions of HTF have higher temperature, but for $c = 4$ mm, regions near the receiver wall have higher temperature. Consequently, as *c* increases, thermal efficiency is improved. However, fluid-fin interaction triggers to generate circular flows and turbulent eddies that enhance pressure loss.

6. Conclusions

A numerical model was introduced to assess the thermal and frictional performance of a PTSC equipped with helical fins and using Cu-Therminol oil VP1 nanofluids as the heat transfer fluid (HTF). The *k*-ε turbulence model was employed to simulate turbulent eddies and circular flows around the fins. Additionally, radiation was modelled using the discrete ordinates method. Conjugate heat transfer among the fins and HTF, HTF and the receiver's inner wall, evacuated air and glass cover, and evacuated air and the receiver's outer wall was also considered. Following experimental validation, the results obtained were as follows:

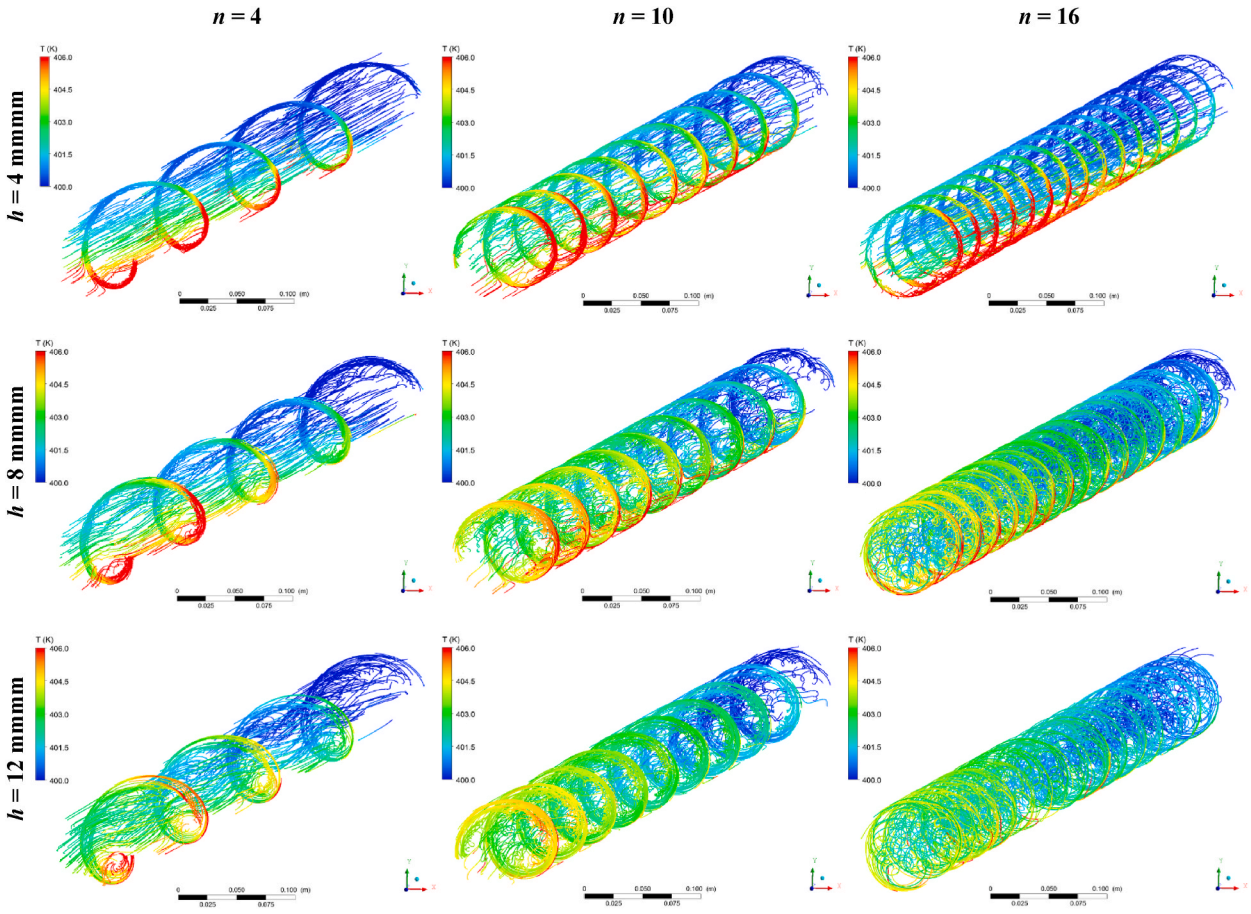

Fig. 11. Changes of flow path patterns with the helical fin turns and heights for $T_{in} = 400$ K, $\varphi_{Cu} = 0.04$, and $Re = 10^5$.

- To avoid excessive pressure losses, fin insertion is recommended for $Re > 3 \times 10^5$ to have a moderate friction factor increment of ~30 %.
- For Reynolds numbers below 5×10^6, helical fins with 10 turns yield the highest thermal efficiency and Nusselt number values, followed by fins with 4 and 16 turns. For instance, at $Re = 10^5$ and a fin height of 8 mm, changing the number of turns from 16 to 4 and 10 results in η increases of 1.6 % and 2.0 %, respectively. The corresponding improvements in Nu are 33 % and 55 %.
- As fin turns increases to 16, the pumping demand significantly increase due to strong circular flows and turbulent eddies near the fin surface. For instance, in $Re = 10^5$, for 8 mm helical fins, as n changes from 16 to 4 and 10, f decreases by 64 % and 54 %, respectively.
- At $Re = 5 \times 10^6$, where axial forced convection is sufficient to transfer absorbed solar heat from the receiver tube wall to the HTF bulk, the thermal efficiency for cases with 16 turns surpasses that of cases with 4 turns. For instance, with a fin height of 12 mm, increasing the number of turns from 4 to 16 enhances thermal efficiency by 1.1 %, although this also results in a significant friction factor increase of 242.4 %.
- Fin height enhancement results in thermal efficiency increment, but the pressure losses are elevated. For example, for $n = 10$, as h increases from 4 mm to 12 mm, the maximum Nu, η and f increments are 18.3 %, 1.9 % and 43.4 %.

To build upon the current study, it is suggested to develop a parabolic trough solar collector featuring helical internal fins and a rotating receiver tube. The rotation of the receiver tube could enhance thermal mixing resulted from the helical inserts, potentially boosting the thermal efficiency of the PTSC. Additionally, incorporating phase change materials with the collector tube could elevate the outflow temperature during periods of low sunlight.

CRediT authorship contribution statement

Guoliang Hou: Writing – original draft, Methodology, Investigation, Supervision. **Anupam Yadav:** Conceptualization, Resources, Validation. **Eyhab Ali:** Writing – original draft, Software, Formal analysis. **Youssef Ali Naeem:** Writing – review & editing, Resources, Visualization. **Fadwa Fathallah Ahmed:** Conceptualization, Formal analysis, Methodology. **Khursheed Muzammil:** Funding acquisition, Methodology, Formal analysis, Validation. **Khaldoon T. Falih:** Writing – Original draft, Visualization, Resources. **Hussam**

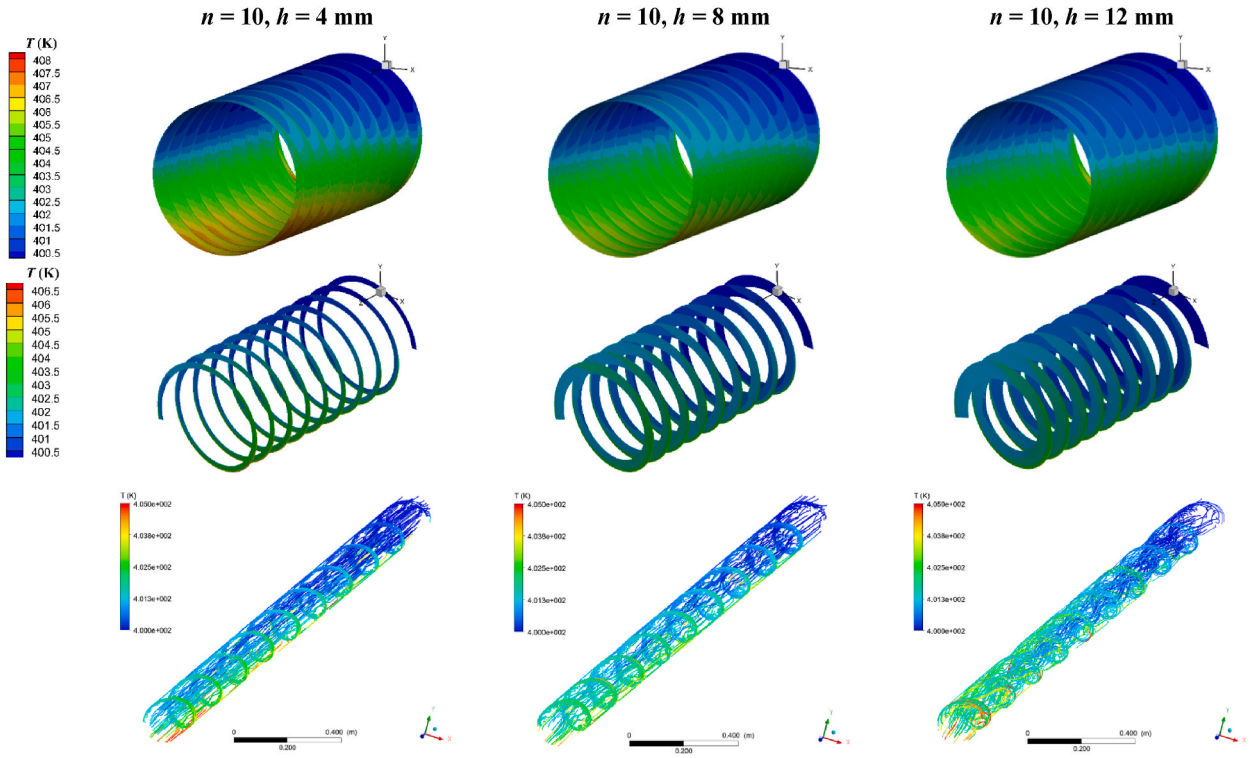

Fig. 12. The effects of c on temperature contours through outer wall and helical fin of the receiver tube and flow path for the following conditions: $T_{in} = 400$ K, $\varphi_{Cu} = 0.04$, and $Re = 3 \times 10^5$.

Abdali Abdulridui: Software, Visualization, Conceptualization. **Eftikhaar Hasan Kadhum:** Writing – review & editing, Methodology, Investigation. **Alaa A. Omran:** Formal analysis, Writing – review & editing, Validation. **Ahmed Elawady:** Writing – review & editing, Validation, Investigation.

Declaration of competing interest

The authors declare that they have no known competing financial interests or personal relationships that could have appeared to influence the work reported in this paper.

Data availability

Data will be made available on request.

Acknowledgements

Changchun Normal University Doctoral Research Startup Fund Project. The authors thank the Deanship of Scientific Research and Graduate Studies at King Khalid University, KSA, for funding this work through a research group program under grant number RGP.2/220/45.

References

[1] M.J. Blanco, S. Miller, Introduction to concentrating solar thermal (CST) technologies, Adv. Conc. Sol. Therm. Res. Technol. (2017) 3–25. Elsevier.
[2] C. Suresh, R.P. Saini, Review on solar thermal energy storage technologies and their geometrical configurations, Int. J. Energy Res. 44 (2020) 4163–4195.
[3] Y\ilmaz, Ibrahim Halil, A. Mwesigye, Modeling, simulation and performance analysis of parabolic trough solar collectors: a comprehensive review, Appl. Energy 225 (2018) 135–174.
[4] S.E. Ghasemi, A.A. Ranjbar, Thermal performance analysis of solar parabolic trough collector using nanofluid as working fluid: a CFD modelling study, J. Mol. Liq. 222 (2016) 159–166.
[5] G.K. Manikandan, S. Iniyan, R. Goic, Enhancing the optical and thermal efficiency of a parabolic trough collector–A review, Appl. Energy 235 (2019) 1524–1540.
[6] E. Bellos, C. Tzivanidis, A review of concentrating solar thermal collectors with and without nanofluids, J. Therm. Anal. Calorim. 135 (2019) 763–786.
[7] V.S. Chara-Dackou, D. Njomo, R. Tchinda, Y.S. Kondji, M.H. Babikir, H.C. Noume, et al., Sensitivity analysis of the thermal performance of a parabolic trough concentrator using Al2O3 and SiO2/Vegetable oil as heat transfer fluid 10 (2024).
[8] S. Damarseckin, A. Atiz, M. Karakilcik, Solar pond integrated with parabolic trough solar collector for producing electricity and hydrogen, Int. J. Hydrogen Energy 52 (2024) 115–126.

[9] Al-Aloosi W, Hamzah H, Others. Thermal performance analysis in a parabolic trough solar collector with a novel design of inserted fins. Hudhaifa, Therm Perform Anal a Parabol Trough Sol Collect with a Nov Des Inser Fins n.d.
[10] P. Liu, N. Zheng, Z. Liu, W. Liu, Thermal-hydraulic performance and entropy generation analysis of a parabolic trough receiver with conical strip inserts, Energy Convers. Manag. 179 (2019) 30–45.
[11] S.E. Ghasemi, A.A. Ranjbar, Numerical thermal study on effect of porous rings on performance of solar parabolic trough collector, Appl. Therm. Eng. 118 (2017) 807–816.
[12] K.A. Ahmed, E. Natarajan, Thermal performance enhancement in a parabolic trough receiver tube with internal toroidal rings: a numerical investigation, Appl. Therm. Eng. 162 (2019) 114224.
[13] B. Jalili, N. Aghaee, P. Jalili, D.D. Ganji, Novel usage of the curved rectangular fin on the heat transfer of a double-pipe heat exchanger with a nanofluid, Case Stud. Therm. Eng. 35 (2022) 102086.
[14] A. Uniyal, Y.K. Prajapati, L. Ranakoti, P. Bhandari, T. Singh, B. Gangil, et al., Recent advancements in evacuated tube solar water heaters: a critical review of the integration of phase change materials and nanofluids with ETCs, Energies 15 (2022) 8999.
[15] H. Singh, T. Alam, M.I. Haque Siddiqui, M. Ashraf Ali, D. Sagar, Experimental investigation of heat transfer augmentation due to obstacles mounted in solar air heater duct, Exp. Heat Tran. 37 (2024) 162–181.
[16] Kumar Gupta N. Karmveer, M.I.H. Siddiqui, D. Dobrot\ua, T. Alam, M.A. Ali, et al., The effect of roughness in absorbing materials on solar air heater performance, Materials 15 (2022) 3088.
[17] B.P. Singh, V.S. Bisht, P. Bhandari, K.S. Rawat, Thermo-fluidic modelling of a heat exchanger tube with conical shaped insert having protrusion and dimple roughness, Aptisi Trans Technopreneursh 3 (2021) 127–143.
[18] J. Singh, V.S. Bisht, P. Bhandari, K. Kumar, J. Singh, T. Alam, et al., Computational parametric investigation of solar air heater with dimple roughness in S-shaped pattern, Int. J. Interact. Des. Manuf. (2023) 1–11.
[19] S. Zhu, Z. Hu, C. Cheng, W. Hu, S. Cao, Y. Peng, et al., Effect of the arrangement of longitudinal vortex generators on the performance of a parabolic trough solar collector, J. Mech. Sci. Technol. 38 (2024) 1473–1486.
[20] S. Ghadirijafarbeigloo, A.H. Zamzamian, M. Yaghoubi, 3-D numerical simulation of heat transfer and turbulent flow in a receiver tube of solar parabolic trough concentrator with louvered twisted-tape inserts, Energy Proc. 49 (2014) 373–380.
[21] C. Chang, C. Xu, Z.Y. Wu, X. Li, Q.Q. Zhang, Z.F. Wang, Heat transfer enhancement and performance of solar thermal absorber tubes with circumferentially non-uniform heat flux, Energy Proc. 69 (2015) 320–327.
[22] X. Zhu, L. Zhu, J. Zhao, Wavy-tape insert designed for managing highly concentrated solar energy on absorber tube of parabolic trough receiver, Energy 141 (2017) 1146–1155.
[23] X. Song, G. Dong, F. Gao, X. Diao, L. Zheng, F. Zhou, A numerical study of parabolic trough receiver with nonuniform heat flux and helical screw-tape inserts, Energy 77 (2014) 771–782.
[24] S. Singh, S. Samir, K. Kumar, Performance analysis of solar parabolic trough receiver with twisted perforated conical inserts, Proc. Inst. Mech. Eng. Part E J Process Mech Eng (2024) 09544089231223001.
[25] B. Mehta, D. Subhedar, Energy, exergy and environmental analysis of concentrated parabolic trough collector using alumina-water nanofluid and twisted tape insert, Proc. Inst. Mech. Eng. Part C J Mech Eng Sci (2024) 09544062241238849.
[26] Halil Y\ilmazIbrahim, A. Mwesigye, T.T. Göksu, Enhancing the overall thermal performance of a large aperture parabolic trough solar collector using wire coil inserts, Sustain. Energy Technol. Assessments 39 (2020) 100696.
[27] H.M. cSahin, E. Baysal, A.R. Dal, N. cSahin, Investigation of heat transfer enhancement in a new type heat exchanger using solar parabolic trough systems, Int. J. Hydrogen Energy 40 (2015) 15254–15266.
[28] B. Kur\csun, Thermal performance assessment of internal longitudinal fins with sinusoidal lateral surfaces in parabolic trough receiver tubes, Renew. Energy 140 (2019) 816–827.
[29] O. Chakraborty, S. Roy, B. Das, R. Gupta, Computational analyses of parabolic trough solar collector in the presence of helical coil-insert, Int. J. Environ. Sci. Technol. 20 (2023) 683–702.
[30] M. Suliman, M. Ibrahim, T. Saeed, Improvement of efficiency and PEC of parabolic solar collector containing EG-Cu-SWCNT hybrid nanofluid using internal helical fins, Sustain. Energy Technol. Assessments 52 (2022) 102111.
[31] S. Thapa, S. Samir, K. Kumar, A review study on the performance of a parabolic trough receiver using twisted tape inserts, Proc. Inst. Mech. Eng. Part E J Process Mech Eng 236 (2022) 699–711.
[32] B. Stanek, J. Ochmann, D. W\kecel, Ł. Bartela, Study of twisted tape inserts Segmental application in low-concentrated solar parabolic trough collectors, Energies 16 (2023) 3716.
[33] P. Jalili, K. Kazerani, B. Jalili, D.D. Ganji, Investigation of thermal analysis and pressure drop in non-continuous helical baffle with different helix angles and hybrid nano-particles, Case Stud. Therm. Eng. 36 (2022) 102209.
[34] M.S. Nazir, A. Shahsavar, M. Afrand, M. Ar\ic\i, S. Nižetić, Z. Ma, et al., A comprehensive review of parabolic trough solar collectors equipped with turbulators and numerical evaluation of hydrothermal performance of a novel model, Sustain. Energy Technol. Assessments 45 (2021) 101103.
[35] M. Zaboli, S.S. Mousavi Ajarostaghi, S. Saedodin, M. Saffari Pour, Thermal performance enhancement using absorber tube with inner helical axial fins in a parabolic trough solar collector, Appl. Sci. 11 (2021) 7423.
[36] T. Oketola, A. Mwesigye, Numerical investigation of the overall thermal and thermodynamic performance of a high concentration ratio parabolic trough solar collector with a novel modified twisted tape insert using supercritical CO2 as the working fluid, Therm. Sci. Eng. Prog. (2024) 102592.
[37] A. Mwesigye, Halil Y\ilmazIbrahim, J.P. Meyer, Numerical analysis of the thermal and thermodynamic performance of a parabolic trough solar collector using SWCNTs-Therminol®VP-1 nanofluid, Renew. Energy 119 (2018) 844–862.
[38] T.L. Bergman, F.P. Incropera, D.P. DeWitt, A.S. Lavine, Fundamentals of Heat and Mass Transfer, John Wiley & Sons, 2011.
[39] A. Mwesigye, Z. Huan, J.P. Meyer, Thermal performance and entropy generation analysis of a high concentration ratio parabolic trough solar collector with Cu-Therminol{®} VP-1 nanofluid, Energy Convers. Manag. 120 (2016) 449–465.
[40] K. Khanafer, K. Vafai, A critical synthesis of thermophysical characteristics of nanofluids, Int. J. Heat Mass Tran. 54 (2011) 4410–4428.
[41] Z. Haddad, H.F. Oztop, E. Abu-Nada, A. Mataoui, A review on natural convective heat transfer of nanofluids, Renew. Sustain. Energy Rev. 16 (2012) 5363–5378.
[42] M. Corcione, Empirical correlating equations for predicting the effective thermal conductivity and dynamic viscosity of nanofluids, Energy Convers. Manag. 52 (2011) 789–793.
[43] S.-Q. Zhou, R. Ni, Measurement of the specific heat capacity of water-based Al 2 O 3 nanofluid, Appl. Phys. Lett. 92 (2008) 93123.
[44] A. Mwesigye, J.P. Meyer, Optimal thermal and thermodynamic performance of a solar parabolic trough receiver with different nanofluids and at different concentration ratios, Appl. Energy 193 (2017) 393–413.
[45] D.B. Spalding, A novel finite difference formulation for differential expressions involving both first and second derivatives, Int. J. Numer. Methods Eng. 4 (1972) 551–559.
[46] S.E. Ghasemi, A.A. Ranjbar, Effect of using nanofluids on efficiency of parabolic trough collectors in solar thermal electric power plants, Int. J. Hydrogen Energy 42 (2017) 21626–21634.
[47] E. Bellos, C. Tzivanidis, D. Tsimpoukis, Enhancing the performance of parabolic trough collectors using nanofluids and turbulators, Renew. Sustain. Energy Rev. 91 (2018) 358–375.
[48] O. Mahian, L. Kolsi, M. Amani, P. Estellé, G. Ahmadi, C. Kleinstreuer, et al., Recent advances in modeling and simulation of nanofluid flows-part II: applications, Phys. Rep. (2018).
[49] A. Fluent, Fluent 14.0 User's Guide, ANSYS FLUENT Inc, 2011.